PNAS NEXUS

PNAS Nexus, 2025, **4**, pgae573

https://doi.org/10.1093/pnasnexus/pgae573
Advance access publication 26 December 2024
Research Report

Physiologic and structural characterization of desisobutyryl-ciclesonide, a selective glucocorticoid receptor modulator in newborn rats

Juliann D. Jaumotte[a], Nathalie El Khoury[a], Charles K. Min[b,c], Jiefei Wang[d], Caroline Madigan[a], Antalya Jano[a], Robin J. Russo Kobylski[b,c], Laura A. Solt[b,c], Rutu S. Dhavan[e], Kelly L. Short[e], Tianhua Lei[f], Uma Chandran[d], Timothy J. Cole[e], Ann Paula Monaghan-Nichols[f], Venkatesh Sampath[g], René Houtman[h], Kendall W. Nettles[b] and Donald B. DeFranco[a,*]

[a]Department of Pharmacology and Chemical Biology, University of Pittsburgh School of Medicine, 3501 Fifth Avenue, Pittsburgh, PA 15261, USA
[b]Department of Immunology and Microbiology, The Herbert Wertheim UF Scripps Institute for Biomedical Innovation & Technology, Jupiter, FL 33458, USA
[c]The Skaggs Graduate School of Chemical and Biological Sciences, The Scripps Research Institute, La Jolla, CA 92037, USA
[d]Department of Biomedical Informatics, University of Pittsburgh, Pittsburgh, PA 15206, USA
[e]Department of Biochemistry and Molecular Biology, Biomedical Discovery Institute, Monash University, Clayton, VIC 3800, Australia
[f]Department of Biomedical Sciences, University of Missouri Kansas City School of Medicine, Kansas City, MO 64108, USA
[g]Department of Pediatrics/Division of Neonatology, Children's Mercy, University of Missouri Kansas City School of Medicine, Kansas City, MO 64108, USA
[h]Department of Research and Development, Precision Medicine Lab, Oss 5349, The Netherlands
*To whom correspondence should be addressed: Email: dod1@pitt.edu
Edited By Ivet Bahar

Abstract

Bronchopulmonary dysplasia, the most prevalent chronic lung disease of prematurity, is often treated with glucocorticoids (GCs) such as dexamethasone (DEX), but their use is encumbered with several adverse somatic, metabolic, and neurologic effects. We previously reported that systemic delivery of the GC prodrug ciclesonide (CIC) in neonatal rats activated glucocorticoid receptor (GR) transcriptional responses in lung but did not trigger multiple adverse effects caused by DEX. To determine whether limited systemic metabolism of CIC was solely responsible for its enhanced safety profile, we treated neonatal rats with its active metabolite desisobutyryl-ciclesonide (Des-CIC). DEX but not Des-CIC caused a reduction in body weight as well as reduced insulin-like growth factor-1 serum levels and chronic hyperglycemia in neonatal rats. However, Des-CIC was as effective as DEX in reducing the expression of various bleomycin-induced proinflammatory cytokine mRNAs. In vitro studies with various cell types demonstrate the potent GR transactivation and transrepression activity of Des-CIC, although genome-wide transcriptomic analyses reveal differences in DEX vs. Des-CIC responses in neonatal rat lung and liver tissue. Des-CIC is a GR super-agonist as revealed by an in vitro coregulator peptide binding assay. In addition, molecular dynamics simulations revealed unique Des-CIC-dependent allosteric signaling pathways between specific residues in the GR ligand-binding domain and receptor surfaces interacting with coregulator peptides. Thus, Des-CIC is a potential novel selective GR modulator that could impart a favorable therapeutic index for CIC use for even modest durations of GC exposure which could have long-lasting adverse somatic, metabolic, or neurologic effects.

Keywords: glucocorticoid receptor, neonate, desisobutyryl-ciclesonide

Significance Statement

Preterm birth significantly increases the risk for bronchopulmonary dysplasia (BPD), a condition associated with long-term pulmonary insufficiency. Synthetic glucocorticoids (sGCs) such as dexamethasone (DEX) are used to prevent BPD but encumber serious adverse effects. In this study, we demonstrate that desisobutyryl-ciclesonide (Des-CIC), a sGC, has limited adverse somatic and metabolic effects but is as effective as DEX in reducing proinflammatory cytokine gene expression in neonatal rat lungs exposed to bleomycin. Molecular dynamics and coregulator peptide interaction studies demonstrated unique interactions and allostery within the glucocorticoid receptor (GR) ligand-binding domain for Des-CIC compared to DEX. Thus, Des-CIC is a selective GR modulator that may be a safer sGC for postnatal treatment of neonatal lung diseases such as BPD.

Competing Interest: The authors declare no competing interests.
Received: July 30, 2024. **Accepted:** December 12, 2024

Introduction

Infants born before 30 weeks gestation are at risk of developing bronchopulmonary dysplasia (BPD), a prevalent chronic lung disease of prematurity (1, 2). Typically, lung inflammation and injury induced by exposure to hyperoxia, infection, mechanical ventilation in the immature lung impairs lung development and causes alveolar remodeling characteristic of BPD (1, 3, 4). Glucocorticoids (GCs) such as dexamethasone (DEX) and budesonide (BUD) have been a mainstay of BPD prevention and treatment as they reduce lung inflammation and injury (5). However, their use is encumbered with several adverse effects including hyperglycemia, impaired somatic and brain growth, cerebral palsy, and long-term neurologic and behavioral disorders (6, 7). These major concerns have resulted in the American Academy of Pediatrics recommending caution and selective use of GC use in preterm infants (8) and heightened the critical need for development of therapeutic GCs that maintain antiinflammatory properties but with limited systemic adverse effects in the neonate during the perinatal period.

Ciclesonide (CIC), an inhaled GC prodrug approved for the treatment of asthma and allergic rhinitis in children and adults (9), is converted to the potent glucocorticoid receptor (GR) agonist desisobutyryl-ciclesonide (Des-CIC) by enzymes enriched in the airways (10). We previously reported that systemic delivery of CIC in neonatal rats activated GR transcriptional responses in lung but did not trigger the adverse effects on somatic growth, brain weight, or cerebral white matter loss caused by DEX leading us to propose CIC as a potential safer GC pharmacotherapy for BPD (11). In support of CIC's potential to limit pathophysiologic events in the lung beyond asthma, we have recently reported that Toll-like receptor 2-mediated acute lung injury and inflammation in neonatal mice induced by SARS-CoV-2 E protein was inhibited by systemic administration of CIC (12).

To determine whether limited systemic metabolism of CIC in neonatal rats was solely responsible for its enhanced safety profile and lung protective effects, we examined the in vivo and in vitro biological activity of Des-CIC, the active metabolite of CIC, which has a higher binding affinity for GR than DEX (13, 14). We also used neonatal rat tissues, primary cell cultures, and established cell lines to compare the transcriptional responses of DEX and Des-CIC. Furthermore, molecular dynamics simulation (MDS) and in vitro coregulator peptide assays provided mechanistic insights into the differences in the in vivo and in vitro responses to DEX and Des-CIC. Thus, our results demonstrate that the unique structural features of Des-CIC impart selective GR modulator (SEGRM) activity that could contribute to a favorable therapeutic index of its parent compound CIC for conditions where even modest durations of GC exposure (e.g. neonates) could have long-lasting adverse somatic, metabolic, or neurologic effects.

Results

Unlike DEX, systemic administration of Des-CIC does not trigger adverse systemic effects

The chemical structures for DEX, Des-CIC and BUD shown in figure (Fig. S1; SI Appendix) highlight the major differences between these GCs that exists at C16/C17 of the steroid D-ring. Both BUD and Des-CIC have a bis-oxy group linked at this position with an isopropyl hydrocarbon chain (BUD) or cyclopentane extension, respectively, in contrast to the C16 methyl and C17 hydroxyl group present in DEX. Despite this bulky addition at the D-ring, Des-CIC has an approximately 10-fold higher in vitro binding affinity for GR than DEX (13, 14). The high plasma protein binding of CIC and Des-CIC (i.e. ~99% relative to approximately 85% for DEX (15);) and extensive metabolism in liver (13) accounts in part for CIC's safety profile when delivered by inhalation. Furthermore, fatty acid esterification in the lung increases their tissue residency time contributing to CIC's efficacy and once daily dosing regimen in asthma patients (16–18). The $t_{1/2}$ of serum Des-CIC measured after intravenous (i.v.) administration of CIC in humans is 3.5 h (19).

We reasoned that the higher binding affinity of Des-CIC for GR relative to DEX could overcome its pharmacokinetic barriers to systemic action and trigger analogous adverse effects as DEX in neonatal rats. Following subcutaneous (s.c.) administration in adult mice, Des-CIC is readily detected in many organs with the liver being most prominent (20). Accumulation of Des-CIC in mouse lung is much more limited after a single s.c. injection but multiple (i.e. 14) s.c. injections of Des-CIC over a period of 5 days leads to its equivalent accumulation in liver and lung (20). However, unlike DEX, Des-CIC did not trigger growth suppression in neonatal rats following five daily injections (Fig. 1A and B), an outcome observed in premature infants after repeated GC exposure (21), and similar to our previous findings demonstrating a lack of reduced somatic growth after CIC exposure (11). Reduced somatic growth in neonates by DEX (Fig. 1A and B) was likely due to the reduction in insulin-like growth factor-1 (IGF-1) (Fig. 1C), the predominant growth factor impacting neonatal growth (22). Finally, persistent hyperglycemia observed after GC treatment of preterm infants (21, 23), was also observed following DEX treatment in neonatal rats (Fig. 1D). A 5-day exposure to Des-CIC led to a transient, minor increase in blood glucose (Fig. 1D).

Systemic Des-CIC is as effective as DEX at reducing bleomycin-induced cytokine gene expression in neonatal rat lung

To determine whether systemic Des-CIC could activate GR in lung and reduce some pathologic features associated with chronic lung disease in preterm infants, we utilized an established model of lung injury in neonatal rats triggered by multiple daily injections with bleomycin from postnatal day 1 (P1) to P11 (Fig. 2A) (24). In this model, DEX and other GCs have been shown to reduce lung injury and inflammation (25).

Bleomycin was effective at inducing robust increases in expression of interleukin (IL)-1β (Fig. 2B) and IL-6 (Fig. 2C) mRNA expression. In this model, Des-CIC was as effective as DEX in suppressing bleomycin induction of IL-1ß (Fig. 2B) and IL-6 (Fig. 2C) and uniquely suppressed expression of tumor necrosis factor alpha (TNFα) (Fig. 2D). GR transactivation activity promoted by Des-CIC in the presence of bleomycin was evident by the induction of major GR target genes *Fkbp5*, *Gilz*, and *Per1* (Figs. S2A–C; SI Appendix). Despite causing lung injury, our bleomycin treatment paradigm did not suppress somatic growth (Fig. S2D and E; SI Appendix) or trigger hyperglycemia (Fig. S2F; SI Appendix). Interestingly, unlike the hyperglycemic effects of DEX treatment alone, glucose levels were not elevated in neonatal rats exposed to DEX and bleomycin (Fig. S2F; SI Appendix). We noted that these animals did not have milk in their stomach, so this finding is likely due to their reduced feeding.

The in vivo antiinflammatory effects of Des-CIC were corroborated by in vitro studies with the A549 human lung epithelial cell line, which showed equivalent efficacy of DEX and Des-CIC in reducing IL-1β induction of IL-1β (Fig. 2E), IL-6 (Fig. 2F), and IL-8

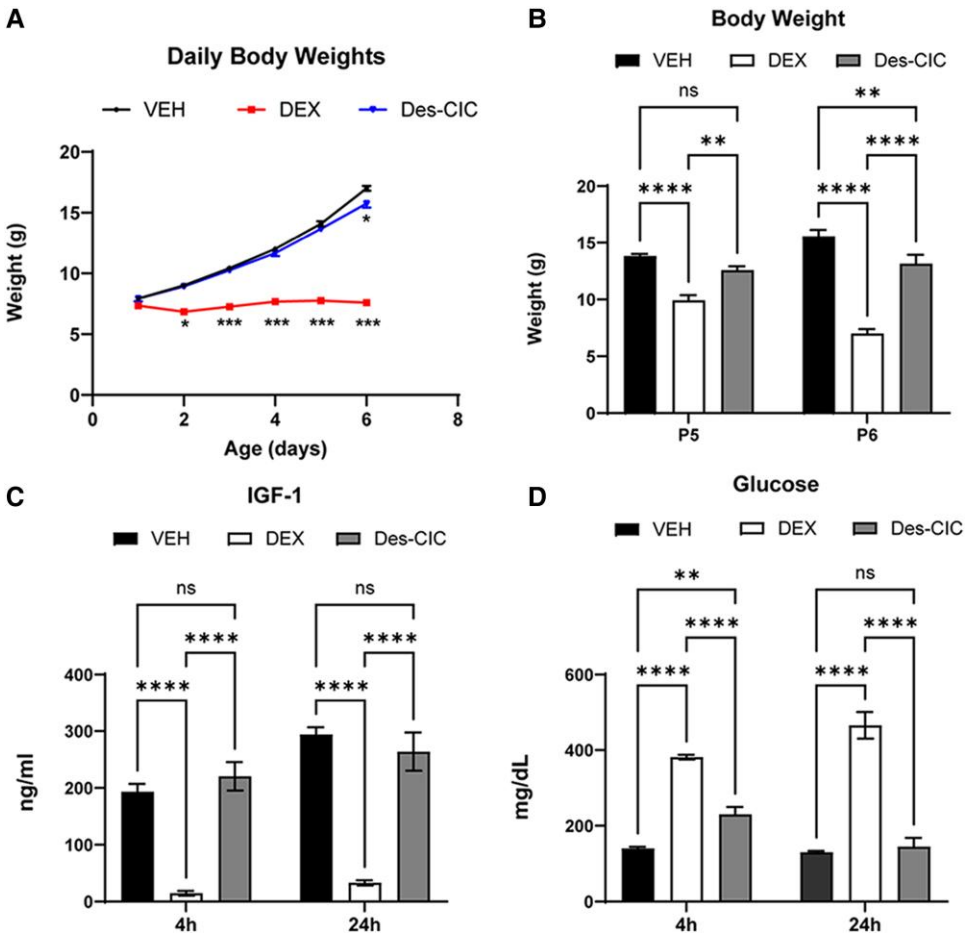

Fig. 1. Differential effects of DEX and Des-CIC on growth and metabolism of neonatal rats. A) Daily weights of neonatal rats treated once daily with vehicle (VEH), DEX (0.5 mg/kg), or Des-CIC (1.25 mg/kg) ($n = 6$ per group). B) Body weight in grams prior to sacrifice at P5 (4 h following final treatment) or P6 (24 h following final treatment) ($n = 4$–8 per group). C) Serum IGF-1 levels as determined by ELISA at 4 h (P5) or 24 h (P6) following final treatment ($n = 5$–9 per group). D) Blood glucose levels at 4 h (P5) or 24 h (P6) following final treatment ($n = 5$–8 per group). All data are expressed as mean ± SEM. Statistical significance was calculated in (A) by two-way ANOVA with repeated measures followed by Dunnett's test post hoc at the daily time points. In (B–D), statistical significance was determined by two-way ANOVA with Bonferroni post hoc test. $^{*}P < 0.05$, $^{**}P < 0.01$, $^{***}P < 0.001$, $^{****}P < 0.0001$.

(Fig. 2G). We also tested antiinflammatory effects in activated mouse $CD8^{+}$ T cells and observed suppression of TNFα and interferon gamma (IFNγ) protein by DEX and Des-CIC (Fig. 2H–J).

Comparison of DEX vs. Des-CIC regulated transcriptome in neonatal rat lung and embryonic mouse lung fibroblasts

Bulk RNA-seq analysis was performed to gain a more comprehensive assessment of Des-CIC transcriptional effects in neonatal rat lung. Given the predominant accumulation of s.c. administered Des-CIC in mouse liver (20) and the likely role of the liver in adverse effects of systemic DEX (i.e. hyperglycemia, reduced serum IGF-1; Fig. 1), we also performed bulk RNA-seq analysis of whole liver. As shown by principal component analysis, the Des-CIC and DEX transcriptomes were markedly different in neonatal rat lung (Fig. 3A) and liver (Fig. 3B) although they were many overlapping responsive genes, particularly in the lung. Specifically, there were 653 genes commonly regulated in the same direction by Des-CIC and DEX (Fig. S3A; SI Appendix) with 300 and 3,169 genes uniquely responsive to Des-CIC and DEX, respectively, in neonatal rat lung (Fig. S3A; SI Appendix). Unsupervised clustering analysis identified a group of 73 genes that had the highest degree of similarity in their response to DEX and Des-CIC in neonatal rat lung (Fig. 3C and D). The two most significant pathways predicted by Reactome to be associated with these 73 genes were involved in surfactant metabolism (Fig. S3C; SI Appendix). Deficiencies in surfactant protein levels are a common pathology in premature infants requiring mechanical ventilation (26). The neonatal liver was much less responsive to Des-CIC with only 204 differentially responsive genes in common with DEX treated animals with 194 and 2,985 genes uniquely responsive to Des-CIC and DEX, respectively (Fig. S3B, SI Appendix). A volcano plot depicting the unique regulated genes in lung and liver (Fig. S3D; SI Appendix) highlights the higher response of lung vs. liver to systemic Des-CIC treatment of neonates.

Late fetal and neonatal lung mesenchymal cells play a major role in the lung maturation properties of GCs (27–29), a feature of relevance to the immature lung of premature infants (30). To compare the DEX and Des-CIC transcriptional response in single cell type that promotes lung maturation, we performed genome-wide microarray transcriptome analysis with mouse primary fetal (i.e. E18.5) lung fibroblasts (PFLF) cell cultures (31) following treatment with saturating concentrations of DEX and Des-CIC (i.e. 1 μM). As shown in the heatmap, there was a high degree of similarity in the most highly upregulated (Fig. 3E) and downregulated (Fig. 3F) genes in DEX vs. Des-CIC treated PFLFs although there are unique genes in the PFLFs that are responsive to DEX

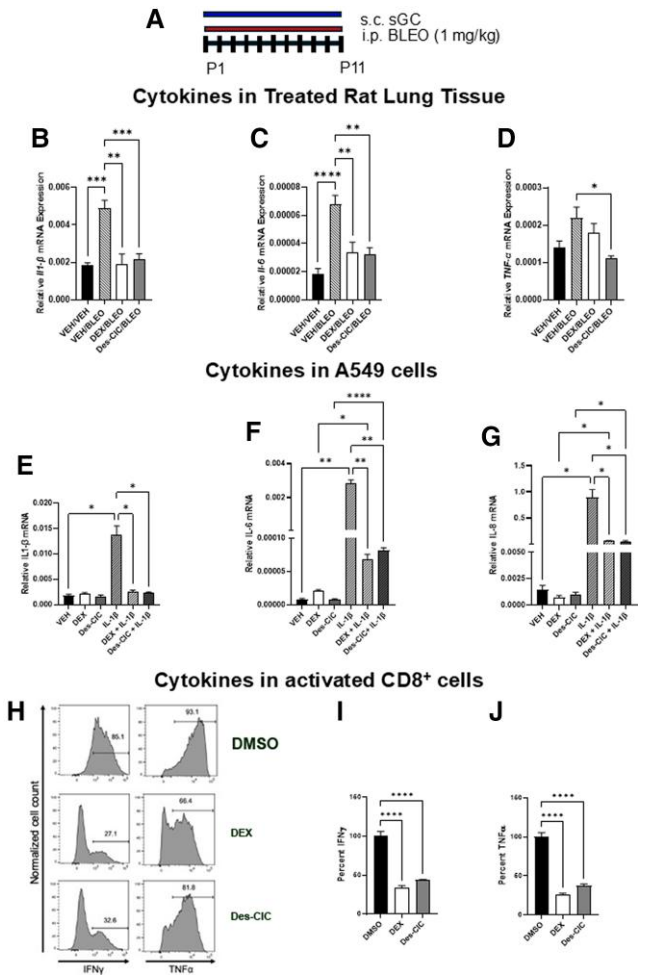

Fig. 2. DEX and Des-CIC suppression of proinflammatory cytokine gene expression. A) Paradigm for neonatal rats treated daily with VEH, DEX (0.1 mg/kg), or Des-CIC (1.25 mg/kg) s.c. before i.p. injection of bleomycin (BLEO) (1 mg/kg) for 11 consecutive days. Relative mRNA expression levels for B) *Il-1β*, C) *Il-6*, and D) *Tnfα*, compared to *Actb* in lung tissue of treated animals ($n = 7$–9 per group). All data are expressed as mean ± SEM. Relative mRNA expression levels for IL-1β (E), IL-6 (F), and IL-8 (G) compared to glyceraldehyde-3-phosphate dehydrogenase in A549 cells exposed to various treatments ($n = 5$ per group). All data are expressed as mean ± SEM. For data in (B–G), statistical significance was determined by Brown–Forsythe and Welch ANOVA tests with Dunnett's T3 post hoc test. $^{*}P < 0.05$, $^{**}P < 0.01$, $^{***}P < 0.001$, $^{****}P < 0.0001$. (H–J) Naïve CD8^{+} T cells from C57BL/6 mice were differentiated into effector-like cells in the presence of vehicle (DMSO), 1 μM DEX, or 1 μM Des-CIC for the final 24 h in culture. T cells were analyzed for the expression of IFNγ and TNFα from single, live cells by flow cytometry. Flow data from a representative experiment are shown in (H) with summary data shown in (I) and (J) for IFNγ and TNFα, respectively
($n = 5$ per group). Data in (I) and (J) are expressed in mean ± SEM. Statistical significance was determined by ANOVA followed by Dunnett's multiple comparison test, $^{****}P < 0.0001$.

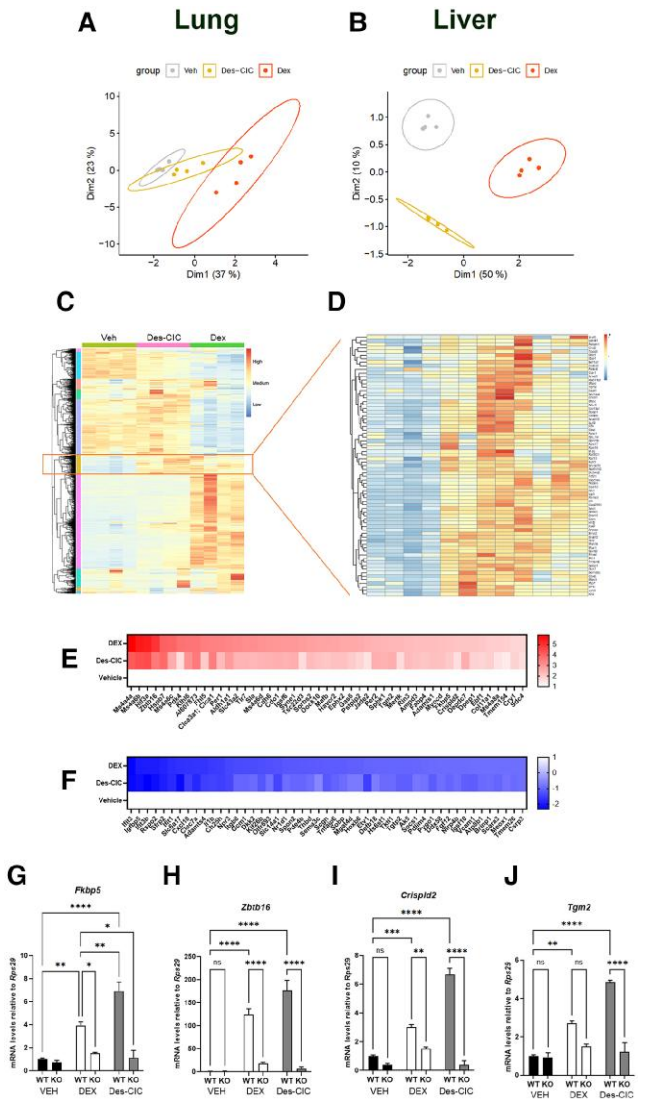

Fig. 3. Des-CIC regulated transcriptome in neonatal rat. Multidimensional scaling plots for gene expression in lung (A) and liver (B). (C) Heatmap showing row-scaled z-scores of normalized gene expression. The hierarchical clustering was performed for top 1,000 variable genes across all lung samples. The genes with similar response to Des-CIC and DEX are highlighted in (D) (see Fig. S3C for the gene sets enrichment in Reactome). Heatmaps from microarray analysis showing the top 50 upregulated (E) and top 50 down regulated (F) mRNAs in cultured mouse primary fetal lung fibroblasts (PFLFs) treated with DEX and Des-CIC for 6 h. Analysis of mRNA levels by RT-qPCR for *Fkbp5* (G), *Zbtb16* (H), *Crispld2* (I), and *Tgm2* (J) in PFLFs treated with VEH, DEX, and Des-CIC for 6 h in cells isolated from both wild-type (WT) and lung mesenchyme-specific GR-KO mice. For data in (G–J) statistical significance was determined by two-way ANOVA followed by Bonferroni multiple comparison test $^{*}P < 0.05$, $^{**}P < 0.01$, $^{***}P < 0.001$, $^{****}P < 0.0001$, $n = 3$ per group.

vs. Des-CIC (Fig. S3E; SI Appendix). This was further illustrated in volcano plots (Fig. S3F; SI Appendix). Analysis of the distribution of fetal lung cell types expressing differentially regulated target genes by DEX vs. Des-CIC showed similar responses in matrix/myofibroblasts and airway epithelium, but a greater response of Des-CIC in distal lung epithelium and vascular endothelial cells (Fig. S3G; SI Appendix). In PFLFs derived from mice with a conditional deletion of the GR gene in lung mesenchyme, induction of prominent GR responsive genes was not observed following treatment with saturating concentrations of DEX or Des-CIC (Fig. 3G–J).

C16/17 substitutions in the D-ring of GCs drive unique structural signaling outcomes

As a probe of surface structure, we applied nuclear receptor affinity profiling (NAPing) (32) to compare the in vitro binding of the GR ligand-binding domain (LBD) in the presence of different GR ligands to a set of immobilized preselected nuclear receptor interacting peptides, including canonical interaction motifs found in coactivators and corepressors. Among these peptides, 58 of them showed at least 2-fold increase in GR binding with DEX treatment, but significantly higher binding with Des-CIC (Fig. 4A).

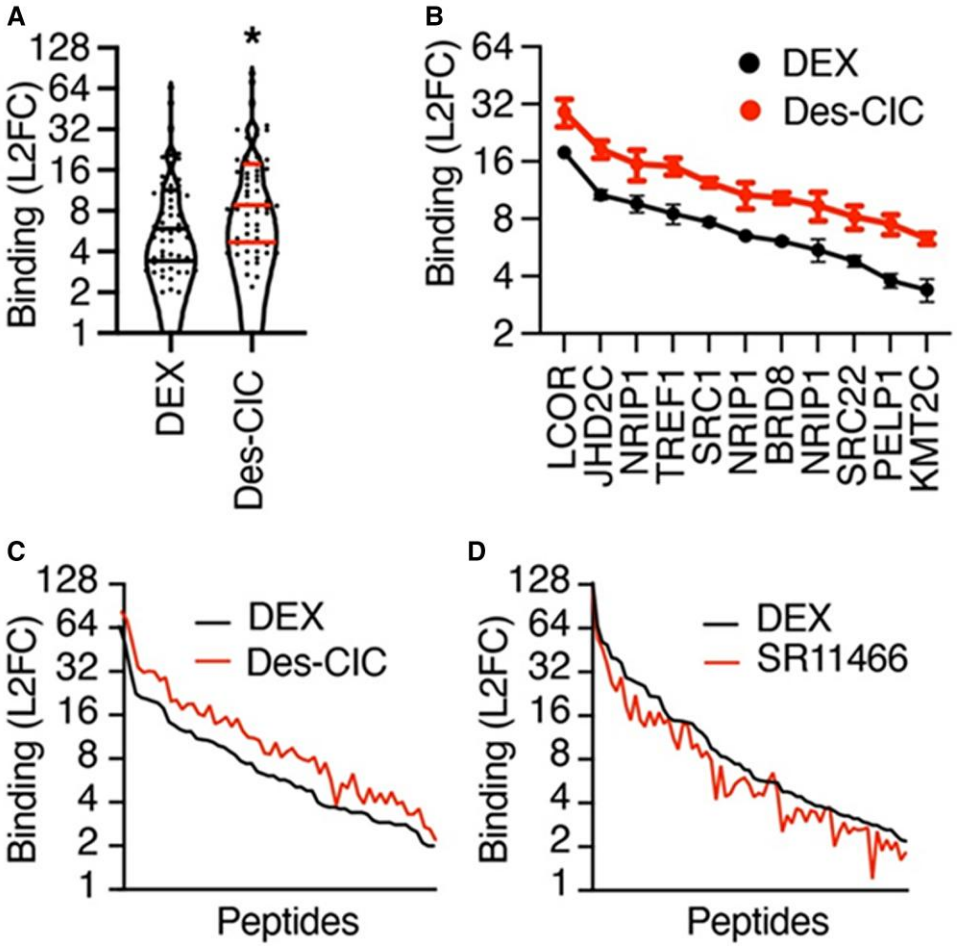

Fig. 4. Des-CIC is a GR super-agonist. A) Violin plots showing in vitro interaction of GR LBD-bound by DEX or Des-CIC with 58 coregulator peptides (i.e. >2 Log_2 fold change). Lines show median and quartiles. L2FC, Log_2 fold change. *Student's paired *t*-test for differences in peptide interactions between DEX vs. Des-CIC bound GR LBD, $P = 1.2 \times 10^{-10}$. B) Selected peptide interactions between DEX vs. Des-CIC bound GR LBD. Mean ± SEM, $n = 3$. C) Individual peptide binding data from (A). D) Peptide binding data of DEX-bound GR LBD compared to binding with a muscle sparing dissociated GC, SR16424 (previously published (33)).

While this assay is a structural probe of ligand pharmacology, several of the peptides with the most super-agonist binding from Des-CIC are also physiologically validated interaction sites, such as the LxxLL amino acid containing peptides from NRIP1, SRC1–2, and PELP1 (Fig. 4B). It is remarkable that all but one of the DEX-interacting peptides showed greater binding to Des-CIC bound GR (Fig. 4C) confirming its super-agonist properties as defined by this in vitro assessment of its function relative to the potent GR agonist, DEX. This contrasts with our previously published results with the selective GR modulator (SEGRM), SR16424, a muscle sparing antiinflammatory GC, which showed many peptides with similar binding as DEX, but a subset with reduced binding (Fig. 4D), further supporting a unique mechanism of action of Des-CIC.

To understand how substitutions to the D-ring C16/17 site of DEX alter the receptor's dynamics, we performed all-atom MDS comparing DEX to Des-CIC and BUD. While the A-ring hydroxyl of DEX formed an H-bond with Q642 in the crystal structure, the cyclohexane of Des-CIC enforced a rotation of Q642 that shifted helix 8 (h8) and induced a flip in Y735 to set up a network of contacts between Des-CIC, Y735, and Q642 (Fig. 5A). In the MDS, we calculated correlation motion networks between Q642 and an LBD-bound SRC-2 peptide and found connections through h5–h6 only for Des-CIC, with no connections for DEX or BUD bound GR LBD at a correlation threshold of 0.3 (Fig. 5B). By reducing the correlation threshold to 0.1, we identified correlated allosteric routes for all three ligands, but Des-CIC induced much shorter pathways (Fig. 5C) that were more directly between Q642 and the bound SRC-2 peptide (Fig. 5D), while DEX and BUD displayed longer path lengths (Fig. 5C) and more diffuse pathways (Fig. 5E and F).

To further study the structural mechanism of Des-CIC selective modulation, we measured ligand induced effects on the h8 backbone position relative to h11 and noted substantial shifts with both BUD and Des-CIC, but significantly greater shifts with Des-CIC compared to BUD (Fig. S4A; SI Appendix). The cyclization of the C16 and C17 with Des-CIC and BUD prevented the H-bond with Q642, but BUD showed a biphasic distribution of Q642 positions relative to the ligand, while with Des-CIC Q642 was uniformly further away (Fig. S4B; SI Appendix). There were also differences in the distribution of Y752 relative to the ligands, with Des-CIC showing greater population of a closer conformer (Fig. S4C; SI Appendix). These observations highlight how relatively small differences between the BUD propyl group and Des-CIC cyclohexane drive conformational differences that are propagated to the coactivator binding surface.

The unique predicted GR LBD conformation adopted in response to Des-CIC relative to BUD binding was surprising given their chemical similarity (i.e. a bis-oxy substitution at C16/17; Fig. S1; SI

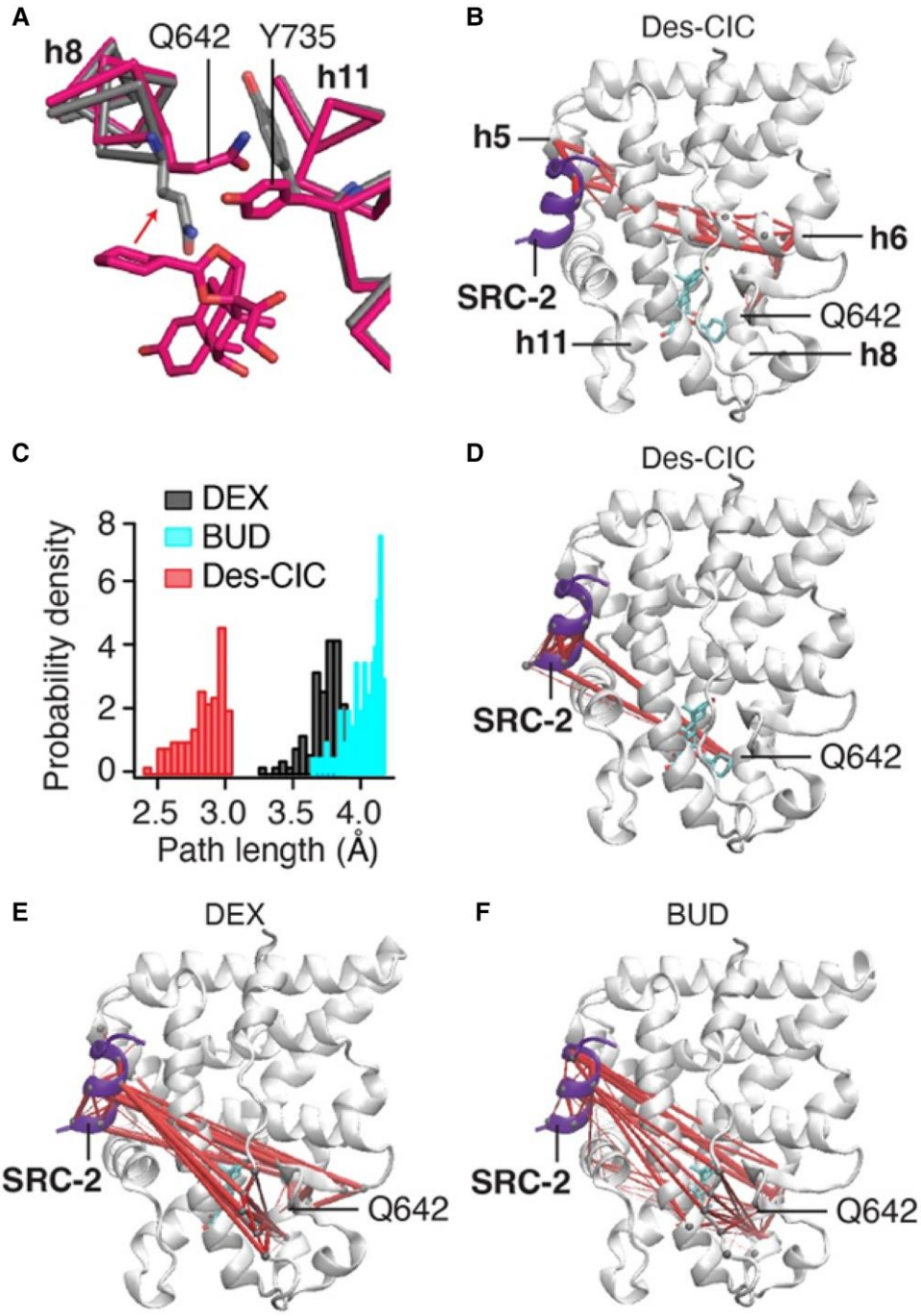

Fig. 5. Structural basis of Des-CIC selectivity in GR LBD conformational changes and allostery. A) Detailed crystal structure of section of GR LBD (pink) bound to Des-CIC (pink) superposed with GR LBD (gray) bound to DEX (not shown). Arrow indicates difference in position of Q642. B) Network analysis of pathways for correlated motion between Q642 and a peptide from the SRC-2 histone acetyl transferase for Des-CIC bound GR LBD. Red edges indicate pathways of allostery with correlation ≥ 0.3, and the weight of the edges signifies strength of correlation. C) Histogram showing suboptimal path lengths with the indicated ligands at correlation threshold ≥0.1. Network analysis of pathways for correlated motion with correlation threshold ≥0.1 with GR LBD occupied by Des-CIC (D), DEX (E), or BUD (F).

Appendix). Des-CIC and BUD also have comparable pharmacokinetic properties in humans (e.g. fatty acid esterification in liver) and therefore may be predicted to have a similar safety profile in preterm infants (34). Thus, we examined various outcomes in neonatal rats given systemic (s.c.) BUD. Surprisingly, unlike Des-CIC but similar to DEX, BUD treatment of neonatal rats led to reduced somatic growth (Fig. S5A and B; SI Appendix) and IGF-1 levels (Fig. S5C; SI Appendix) as well as hyperglycemia (Fig. S5D; SI Appendix). BUD effectively promotes GR transactivation in lung as demonstrated by the induction of *Fkbp5*, *Gilz*, and *Per1* (Fig. S5E–G; SI Appendix).

Discussion

GC pharmacotherapy is widely used for many diseases with an inflammatory component, but their efficacy is often counterbalanced by many adverse side effects (35). Thus, considerable

resources and studies have been devoted to the development of SEGRMs, which would maintain potent antiinflammatory action but have limited systemic adverse effects. While some SEGRMs have progressed to clinical trials (35–38), none have been approved for use in humans except for the partial agonist vamorolone for the treatment of adults and children with Duchenne's muscular dystrophy (39). The efficacy and safety profile of vamorolone is a result of its potent transcription repression properties but limited ability to transactivate GR, features of a classically defined "dissociated" GR agonist (40). Detailed structural and in vitro peptide binding assays demonstrated the partial agonist activity of vamorolone (41). Based upon results presented herein, we propose that Des-CIC could have SEGRM activity and provide an effective pharmacotherapeutic option for chronic lung disease in preterm infants with a safety profile that exceeds the current GCs commonly used in this population, i.e. DEX and BUD. The induction of proinflammatory cytokines by treatment of neonatal rats with bleomycin is abolished to the same extent by coincident systemic Des-CIC or DEX treatment. However, the adverse effects of DEX in neonatal rats that mimic those observed in preterm infants treated with GCs, i.e. hyperglycemia, and growth suppression (6, 7), were not triggered by Des-CIC.

Des-CIC is currently not an approved FDA drug for systemic treatment but the prodrug from which it is derived, CIC, is approved for use in children either by inhalation for asthma or by intranasal delivery for allergic rhinitis (9). The organ restricted metabolism of CIC (10) and its limited bioavailability (13, 15) provides one level of safety that could allow for effective antiinflammatory doses of CIC to be delivered by inhalation (42) to preterm infants to prevent and or treat emerging BPD and prove more effective than inhaled GCs used to date, which have either not proven to be particularly effective for BPD treatment (43) or associated with increased mortality (44). The ability of Des-CIC to bind to or activate the mineralocorticoid receptor has not been tested but seems unlikely given the similarity between Des-CIC and DEX within the steroid A-ring (i.e. double bond between C1/C2), a feature that distinguishes DEX from cortisol, a GR agonist that also binds and activates the mineralocorticoid receptor. Furthermore, the clinical preparation of CIC (i.e. Alvesco) has not been found to have any mineralocorticoid activity in humans (https://www.accessdata.fda.gov/drugsatfda_docs/label/2012/021658s006lbl.pdf).

Although BUD and Des-CIC have very similar chemical structures (i.e. bis-oxy modification at C16/17) as well as physical chemical and pharmacokinetic properties (45), the MDS data reveal a distinction in their impact on the structure and allostery in the GR LBD. Thus, while bulky C16/C17 substitutions on the steroid ring of GCs disrupt a critical H-bond interaction between bound steroid and Q642, the cyclohexane group that extends from the C16/C17 bis-oxy group of Des-CIC imparts a unique allosteric potential for protein interactions with the coregulator binding surface of the GR LBD that could contribute to the super-agonist activity of Des-CIC as defined by in vitro coregulator binding assays (32). The fact that the super-agonist activity of Des-CIC does not trigger adverse somatic growth and metabolic effects in neonatal rats suggests that the unique coregulator composition in neonatal cell types impacts how the Des-CIC induced GR LBD structural change is translated to GR transcriptional responses. The markedly different physiologic effects in neonatal rats with hyperglycemia and growth suppression caused by systemic BUD but not Des-CIC illustrates how the unique GR LBD allostery imposed following Des-CIC binding has physiologic consequences that influence its safety profile. We cannot exclude the possibility that nongenomic effects of Des-CIC bound GR could also impact its antiinflammatory properties and limit adverse systemic effects, particularly given the recent demonstration of the role of nongenomic GR action in its antiinflammatory properties (46).

The pharmacokinetic properties of synthetic GCs in human neonates are unknown but could be influenced by low levels of plasma binding proteins relative to adults (47), thereby impacting free GC levels. This may be relevant to results from the recent NEUROSIS clinical trial with inhaled BUD that showed some increased survival without BPD in extremely preterm infants, but increased mortality of BUD treated infants from unknown causes before 2 years of age (44). BUD has limited hepatic metabolism and exhibits systemic absorption even following inhalation delivery (48, 49) with a plasma $t_{1/2}$ of 1.6 h and peak concentration of 0.7 ng/mL (~2 nM; $K_D = 1.32$ nM) in plasma following delivery by inhalation in adult humans (50). Thus, inhaled BUD has the potential to promote adverse metabolic and growth suppression via activation of GR in tissues outside of the lung. However, if our studies in neonatal rats are translatable to premature infants, inhaled CIC may be a safer alternative than BUD to treat or prevent BPD in preterm infants, particularly using modes of delivery currently being evaluated in clinical trials that seek to limit systemic absorption and combine GC treatment with other agents that promote lung function in preterm infants (34). Furthermore, if the SEGRM function of Des-CIC applies beyond the neonatal stage, novel C16/17 modified GCs with similar impact on GR LBD structure and allostery as Des-CIC (or Des-CIC itself) may hold promise for disease states where systemic GCs provide some therapeutic benefit but are limited by numerous adverse side effects.

Materials and methods

Animals

All animal experiments were conducted under the parameters of the *NIH Guide for the Care and Use of Animals* and approved by the Animal Care and Use Committee of the University of Pittsburgh. Timed-pregnant Sprague Dawley rats (*Rattus norvegicus*) (Charles River) were housed individually in standard microisolator cages with free access to food (Prolab Isopro RMH 3000, LabDiet) and water. Within 24 h of birth, pups were weighed individually across all treatment groups. The use of C57Bl/6 mice (*Mus musculus*) for preparation of PFLFs was approved by the Monash University Committee for Ethics in Animal Experimentation, Monash University, Australia.

GC and bleomycin treatment of neonatal rats

Rat pups starting at postnatal day P1 through P5 were administered vehicle (VEH) (2.5% ethanol), 0.1 mg/kg DEX (Sigma), 1.25 mg/kg Des-CIC (Sigma), or 1.25 mg/kg BUD (Sigma) subcutaneously (s.c.) daily at the nape of the neck. Pups were weighed daily prior to injection. For experiments that included bleomycin (Cayman Chemicals), starting at P1 through P11 rat pups were administered VEH, 0.1 mg/kg DEX or 1.25 mg/kg Des-CIC as above, followed by an interparietal injection (i.p) injection of 1 mg/kg bleomycin (25). Tissue was collected 6 h after the last injection on P11. All pups were weighed daily before injections. DEX treated neonates were given additional injections of sterile saline as needed if showing signs of dehydration by using the skin turgor test.

Glucose measurements

Glucose was measured on the day of sacrifice from trunk blood using the Precision Xtra Blood Glucose & Ketone Monitoring System

(Abbott Diabetes Care Inc) and single use test strips. Two to three readings were taken on each animal and the average was used for comparisons. As glucose measurements may be affected by the time of day of the reading, 4 and 6 h readings were always performed in the afternoon when the animals were sacrificed, and the order of the collection was randomized across treatment groups. Total time for tissue collection was 2–3 h per litter. Similarly, the 24 h glucose readings were always performed in the morning.

IGF-1 measurements

IGF-1 level were determined in serum using an ELISA kit in a 96 well format with 5 μL of sample following instructions from the manufacturer (Crystal Chemical).

A549 cell cultures

Human lung epithelial A549 cells (ATCC) were plated at 250,000 in six well plates (Corning Costar) in Dulbecco's Modified Eagle Medium/F12 containing L-glutamine (Corning) supplemented with 10% fetal bovine serum (FBS) (Atlanta Biologicals) and 50 units/mL Penicillin (Sigma) and 0.5 mg/mL streptomycin (Sigma). After 24 h, cells were shifted to media containing 0.1% FBS. The media was changed again after 24 h immediately before treatment. Cultures were treated with vehicle (EtOH), DEX, or Des-CIC to a final concentration of 10^{-7} M for 1 h before the addition of 1 ng/mL IL-1β (Bio-Techne) in 0.1% bovine serum albumin (BSA) and phosphate buffered saline (PBS) for 6 h. The vehicle treated cultures was also incubated with the same volume 0.1% BSA in PBS. After the incubation the media was removed and the cells washed with Dulbecco's phosphate buffered saline-$MgCl_2$, -$CaCl_2$ (Gibco) before RNA was extracted with Trizol (Invitrogen) and gene expression analyzed by RT-qPCR.

Mouse PFLF cultures

For the isolation of PFLFs, lungs were obtained from embryonic day 18.5 (E18.5) wild-type mice and mice with a conditional knockout (KO) of the GR in lung mesenchyme (GRmesKO) (28). The isolation procedure, detailed in previous studies (31, 51), involved harvesting lungs and isolating fibroblasts through differential attachment, resulting in a population comprising 99% fibroblasts cultures. Fibroblast cells from each litter were treated as one biological replicate ($n = 1$). Cells were cultured in Waymouth media supplemented with 10% FBS, 50 U/mL penicillin, and 50 ug/mL streptomycin at 37 °C in 5% CO_2. PFLFs were cultured in Waymouth media containing 10% charcoal stripped FBS as above. Following overnight incubation, cells were treated for 6 h with either VEH (0.01% ethanol), 1 μM of DEX, or 1 μM Des-CIC.

Mouse T-cell isolation and treatment

Seven- to 9-week-old male and female C57BL/6 mice from the Jackson Laboratory (Bar Harbor, ME, USA) were maintained with regular chow and water ad libitum under the guidelines of the UF Scripps Biomedical Research Institutional Animal Care and Use Committee. Naïve CD8+ T cells were isolated from spleens and lymph nodes of mice using the EasySep Mouse Naïve CD8+ T-cell isolation kit (STEMCELL Technologies, Canada, 19858A) following the manufacturer's instructions after removing red blood cells using Lympholyte-M (Cedarlane Laboratories). Cells were cultured as previously described (52) in T-cell medium (Dulbecco's modified Eagle's medium supplemented with 10% FBS, nonessential amino acids, 10 mM 2-[4-(hydroxyethyl)piperazin-1-yl]ethanesulfonic acid, 2 nM L-glutamine, sodium pyruvate, arginine, aspartate, folic acid, 50 μM 2-mercaptoethanol, MEM vitamin solution) at 37 °C in 10% CO_2 in a volume of 200 μL in 96-well U-bottomed plates. After isolation, cells were plated at a density of 2×10^5 cells per well and activated with anti-CD3 (clone 2C11, 1 μg/mL) and anti-CD28 (clone 37.51, 1 μg/mL) by precoating plates with 50 μg/mL goat antihamster IgG (MP 56984). After 48 h, the activated cells were directly resuspended, counted, and re-cultured at a concentration of 1×10^5 cells per well by diluting the cells into fresh media containing 100 U/mL recombinant human IL-2 (NIH); cells were re-cultured daily. On day 5, cells were treated with 1 μM of compound or dimethylsulfoxide (DMSO) (vehicle), and on day 6, they were restimulated with 50 ng/mL phorbol-12-myristate-13-acetate (Sigma) and 1 μg/mL ionomycin (Sigma) for 2 h with the addition of GolgiStop (BD Bioscience) for an additional 2 h before staining. Following staining for viability (eBioscience Fixable eFluor780), cells were fixed and permeabilized using the Foxp3 staining kit (eBioscience) with anti-IFNγ (BioLegend APC clone XMG1.2) and anti-TNFα (Invitrogen PE/Cyanine7 clone MP6-XT22). Staining was performed using fluorescence activated cell sorting buffer (0.5% BSA, 2 mM EDTA in PBS). All flow cytometry data were analyzed using a BD Symphony instrument (BD Biosciences) and FlowJo 10.10.0 software.

RNA isolation and RT-qPCR

RNA was isolated from frozen rat lung and liver by digesting tissue in Trizol (Invitrogen) using a Lysing Matrix in a MP Biomedicals FastPrep-25 5G homogenizer followed by a chloroform extraction. RNA was isolated from A549 cells in Trizol without the use of a homogenizer. cDNA was prepared by using 1,000 ng of RNA per reaction with an iScript cDNA kit (Bio-Rad). qRT-PCR analysis was performed using a Bio-Rad SYBR Master Mix and run on a CFX96 Real-Time System/C1000 Touch thermal cycler using Bio-Rad CFX Manager 3.1 software.

RNA was isolated from PFLFs cultures following the TRIzol (Ambion by Life Technologies, USA) extraction protocol and cDNA prepared using the QuantiTect Reverse Transcription Kit (Qiagen, Germany). qRT-PCR was performed using the 2× QuantiNova SYBR Green PCR Mastermix from Qiagen (Germany) and the CFX96 Real-Time System/C1000 Touch thermal cycler from Bio-Rad (USA) with Bio-Rad CFX Manager 3.1 software used for analysis. Relative normalized mRNA levels were assessed using the ΔΔCT method. A table of primers utilized for this study is provided in the Supplementary material (Table S1; SI Appendix).

RNA-seq analysis: preprocessing

The reverse stranded paired-end RNA-Seq reads were checked for presence of adapters and quality with FastQC (v0.11.9) (http://www.bioinformatics.babraham.ac.uk/projects/fastqc/). The high-quality reads were trimmed for adapters with Cutadapt (v2.10) (https://journal.embnet.org/index.php/embnetjournal/article/view/200). The trimmed reads were mapped against the Ensembl *Rattus norvegicus* reference genome (mRatBN7.2 v107, retrieved on July 2022) (53) with HISAT2 (v2.2.1) (53). The output SAM files from HISAT2 were converted to binary alignment map files using SAMtools (v1.14) (54). Gene counts were generated with HT-Seq (v0.13.5) (55).

Differential expression and downstream analysis

Read counts were subsequently imported into edgeR (v3.36.0) for differential gene expression analysis with R (v4.1.3) (56). Differentially expressed genes were selected with false discovery rate < 0.05 and absolute log2 fold change (lfc) > 1 for comparisons

between two experimental conditions. Hierarchical clustering w/ as performed using the top 1,000 highly variable genes, with Euclidean distance as the metric and "complete" as the method. The genes in the selected clusters were uploaded to Enrichr (maayanlab.cloud/Enrichr) (57) for gene set enrichment and pathway analysis.

The scatter plots, Venn diagrams, volcano plots, heatmaps, and bar plots were generated with venndir (v0.0.21.900) (https://github.com/jmw86069/venndir) Enhanced Volcano (v1.12.0) (https://bioconductor.org/packages/release/bioc/html/EnhancedVolcano.html), pheatmap (v1.0.12) (https://cran.r-project.org/web/packages/pheatmap/index.html) and ggpubr (v0.4.0).

Affymetrix clariom S gene chip protocol

RNA suitable for microarray analysis required an integrity defined by a 260/280 absorption ration of ≥1.8 and RNA integrity value of ≥0.8 determined via a Bioanalyse 2100. In vitro transcription was performed with 100 ng of purified total RNA using the MessageAmp Premier Enhanced assay protocol (Fisher Scientific). Confirmation of cRNA diversity was performed by using a Nanodrop to generate an electrophoretogram for each in vitro transcription reaction regarding sample yield, integrity and size diversity against a reference RNA. Fifteen micrograms of purified, amplified, biotin-labeled cRNA was fragmented and hybridized to an Affymetrix Clariom S chip, washed in a Fluidics Station 450, and scanned using a Scanner 3000 immediately after hybridization according to manufacturer's instructions (ThermoFisher Scientific 00-00079, 00-0210). Scanned microchips (in. Cel format) were imported in Transcription Analysis Software (ThermoFisher Scientific version 2.0) and compared statistically.

Microarray data analysis

Of the 22,206 genes analyzed, differentially regulated genes were selected at a $P < 0.05$ significant fold change compared to controls using transcriptome analysis software (TAC). Data sets were analyzed for significant regulated biological pathways using Ingenuity Pathway Analysis software (Qiagen).

NAPing assay

The NAPing assay was performed as described previously (32) with the glutathione S-transferase-tagged recombinant GR LBD (A15668; Invitrogen) incubated with either 1 μM DEX or Des-CIC.

MDS and analysis

Initial structures used for simulation were built from two GR LBD crystal structures: Protein Data Bank (PDB) 4UDC (DOI: https://doi.org/10.2210/pdb4DUC/pdb) (DEX-bound) and 5NFP (DOI: https://doi.org/10.2210/pdb5NFP/pdb) (all other states). The ligand in 5NFP was stripped and used to dock all other ligands using Autodock Vina (58). Five hundred nanosecond production simulations were run in triplicates for each complex using AMBER as previously discussed (33).

Trajectory postprocessing and analysis was performed with CPPTRAJ (59) and Bio3D (60). The autoimage command was used to recenter trajectory coordinates and strip command was used to remove water and ion molecules. Suboptimal paths between Q642 and the NCoA2 peptide were calculated with the Bio3D cnapath, with 100 paths collected for each pair of nodes analyzed at various correlation thresholds. Paths were visualized and illustrated in VMD.

Statistical analysis

Data analysis was conducted with GraphPad statistical software (Prism, version 9). A one-way or two-way ANOVA for comparison of multiple groups followed by the appropriate post hoc test as indicated (e.g. Dunnett's test, Tukey, Bonferroni). If the Brown–Forsythe indicated significantly unequal variance between groups, a nonparametric Kruskal–Wallis test was used (indicated by H statistic), followed by a Dunnett's post hoc test. For the growth curve, GraphPad version 9 (Prism) was used for two-way ANOVA with repeated measures followed by Bonferonni post hoc at the daily time points. Results are presented as the mean ± SEM.

Supplementary Material

Supplementary material is available at *PNAS Nexus* online.

Funding

Funding comes from the Eunice Kennedy Shriver National Institute of Child Health and Human Development Grant No. R01 HD104215 (J.D.J., N.E.K., J.W., C.M., A.J., U.C., T.H.L. A.P.M.N, V.S., and D.B.D.), the National Institute of General Medical Sciences Grant No. R01 GM146385 (L.A.S. and K.W.N.), the National Heart, Lung and Blood Institute Grant No. R01 HL162937 (V.S.), the University of Missouri Kansas City (A.P.M.N.), an Ideas Grant (#1185813) from the National Health & Medical Research Council of Australia (R.S.D., K.L.S., and T.J.C.).

Author Contributions

J.D.D. collected and analyzed data, planned experiments, wrote and edited initial drafts of manuscript; N.E.K. obtained and analyzed data, planned experiments, wrote and edited initial drafts of manuscripts; C.K.M. collected and analyzed data, planned experiments, wrote and edited initial drafts of manuscript; J.W. analyzed data, wrote and edited initial drafts of manuscript; C.M. collected and analyzed data, planned experiments; A.J. collected and analyzed data, planned experiments; R.J.R.K. collected and analyzed data, planned experiments, wrote and edited initial sections of manuscript; L.A.S. collected and analyzed data, planned experiments, wrote and edited initial sections of manuscript; R.S.D. collected and analyzed data, planned experiments; K.L.S. collected and analyzed data, planned experiments; T.L. analyzed data, wrote and edited multiple drafts of manuscript; U.C. analyzed data, supervised and provided support for J.W., wrote and edited multiple drafts manuscript; T.J.C. analyzed data, supervised and provided support for R.S.D. and K.L.S., wrote and edited multiple drafts of manuscript; A.P.M.N. analyzed data, supervised and provided support for T.L., wrote and edited multiple drafts of manuscript; V.S. aided in initial concept design, edited all drafts of manuscript; R.H.-collected and analyzed data, planned experiments, wrote and edited multiple drafts of manuscript; K.W.N. conceptualized some experimental approaches, analyzed data, supervised and provided support for C.K.M., R.J.R.K., and L.A.S., edited all drafts of manuscript; D.B.D. conceptualized entire study, analyzed data, supervised and provide support for J.D.D., N.E.K., C.M., and A.J., wrote initial draft of manuscript and edited all drafts including the final version of the manuscript.

Data availability

All genome-wide RNA expression data (i.e. RNA-Seq, Affymetrix microarray) has been submitted to Gene Expression Omnibus (GEO), received a token number and awaiting an accession number assignment. Once the manuscript is published the GEO accession numbers for all genome-wide RNA expression data will be shared and available to the public. The programs used to analyze all genome-wide RNA expression data are described in detail and referenced in the Materials and methods section. The codes used for MDS analyses from publicly available protein structures are also described in detail and cited in the Materials and methods section. No unique materials were generated by studies described in this manuscript.

References

1 Thebaud B, *et al.* 2019. Bronchopulmonary dysplasia. *Nat Rev Dis Primers*. 5(1):78.
2 Jensen EA, *et al.* 2021. Severity of bronchopulmonary dysplasia among very preterm infants in the United States. *Pediatrics*. 148(1):e2020030007.
3 Gilfillan M, Bhandari A, Bhandari V. 2021. Diagnosis and management of bronchopulmonary dysplasia. *BMJ*. 375:n1974.
4 Salimi U, Dummula K, Tucker MH, Dela Cruz CS, Sampath V. 2022. Postnatal sepsis and bronchopulmonary dysplasia in premature infants: mechanistic insights into "New BPD". *Am J Respir Cell Mol Biol*. 66(2):137–145.
5 Watterberg K. 2012. Evidence-based neonatal pharmacotherapy: postnatal corticosteroids. *Clin Perinatol*. 39(1):47–59.
6 Ramaswamy VV, *et al.* 2021. Assessment of postnatal corticosteroids for the prevention of bronchopulmonary dysplasia in preterm neonates: a systematic review and network meta-analysis. *JAMA Pediatr*. 175(6):e206826.
7 Jensen EA, *et al.* 2023. Assessment of corticosteroid therapy and death or disability according to pretreatment risk of death or bronchopulmonary dysplasia in extremely preterm infants. *JAMA Netw Open*. 6(5):e2312277.
8 Cummings JJ, Pramanik AK; COMMITTEE ON FETUS AND NEWBORN. 2022. Postnatal corticosteroids to prevent or treat chronic lung disease following preterm birth. *Pediatrics*. 149(6): e2022057530.
9 Pedersen S, *et al.* 2010. Efficacy and safety of three ciclesonide doses vs placebo in children with asthma: the RAINBOW study. *Respir Med*. 104(11):1618–1628.
10 Mutch E, Nave R, McCracken N, Zech K, Williams FM. 2007. The role of esterases in the metabolism of ciclesonide to desisobutyryl-ciclesonide in human tissue. *Biochem Pharmacol*. 73(10): 1657–1664.
11 Jaumotte JD, *et al.* 2021. Ciclesonide activates glucocorticoid signaling in neonatal rat lung but does not trigger adverse effects in the cortex and cerebellum. *Neurobiol Dis*. 156:105422.
12 Menden HL, *et al.* 2023. The SARS-CoV-2 E protein induces toll-like receptor 2-mediated neonatal lung injury in a model of COVID-19 viremia that is rescued by the glucocorticoid ciclesonide. *Am J Physiol Lung Cell Mol Physiol*. 324(5):L722–L736.
13 Christie P. 2004. Ciclesonide: a novel inhaled corticosteroid for asthma. *Drugs Today (Barc)*. 40(7):569–576.
14 Stoeck M, *et al.* 2004. In vitro and in vivo anti-inflammatory activity of the new glucocorticoid ciclesonide. *J Pharmacol Exp Ther*. 309(1):249–258.
15 Ayyar VS, Song D, DuBois DC, Almon RR, Jusko WJ. 2019. Modeling corticosteroid pharmacokinetics and pharmacodynamics, Part I: Determination and prediction of dexamethasone and methylprednisolone tissue binding in the rat. *J Pharmacol Exp Ther*. 370(2):318–326.
16 Nave R, Meyer W, Fuhst R, Zech K. 2005. Formation of fatty acid conjugates of ciclesonide active metabolite in the rat lung after 4-week inhalation of ciclesonide. *Pulm Pharmacol Ther*. 18(6):390–396.
17 Lexmuller K, *et al.* 2007. Differences in endogenous esterification and retention in the rat trachea between budesonide and ciclesonide active metabolite. *Drug Metab Dispos*. 35(10): 1788–1796.
18 Nave R, Watz H, Hoffmann H, Boss H, Magnussen H. 2010. Deposition and metabolism of inhaled ciclesonide in the human lung. *Eur Respir J*. 36(5):1113–1119.
19 Nave R, Bethke TD, van Marle SP, Zech K. 2004. Pharmacokinetics of [14C]ciclesonide after oral and intravenous administration to healthy subjects. *Clin Pharmacokinet*. 43(7):479–486.
20 Mars U, d'Argy R, Hallbeck K, Miller-Larsson A, Edsbacker S. 2013. Tissue accumulation kinetics of ciclesonide-active metabolite and budesonide in mice. *Basic Clin Pharmacol Toxicol*. 112(6):401–411.
21 Filippone M, Nardo D, Bonadies L, Salvadori S, Baraldi E. 2019. Update on postnatal corticosteroids to prevent or treat bronchopulmonary dysplasia. *Am J Perinatol*. 36(S 02):S58–S62.
22 Hellstrom A, *et al.* 2016. Role of insulinlike growth factor 1 in fetal development and in the early postnatal life of premature infants. *Am J Perinatol*. 33(11):1067–1071.
23 Tas E, Garibaldi L, Muzumdar R. 2020. Glucose homeostasis in newborns: an endocrinology perspective. *Neoreviews*. 21(1): e14–e29.
24 Tourneux P, Markham N, Seedorf G, Balasubramaniam V, Abman SH. 2009. Inhaled nitric oxide improves lung structure and pulmonary hypertension in a model of bleomycin-induced bronchopulmonary dysplasia in neonatal rats. *Am J Physiol Lung Cell Mol Physiol*. 297(6):L1103–L1111.
25 Ishikawa S, *et al.* 2023. A glucocorticoid-receptor agonist ameliorates bleomycin-induced alveolar simplification in newborn rats. *Pediatr Res*. 93(6):1551–1558.
26 Ballard PL, *et al.* 2019. Surfactant status and respiratory outcome in premature infants receiving late surfactant treatment. *Pediatr Res*. 85(3):305–311.
27 Habermehl D, *et al.* 2011. Glucocorticoid activity during lung maturation is essential in mesenchymal and less in alveolar epithelial cells. *Mol Endocrinol*. 25(8):1280–1288.
28 Bird AD, Choo YL, Hooper SB, McDougall AR, Cole TJ. 2014. Mesenchymal glucocorticoid receptor regulates the development of multiple cell layers of the mouse lung. *Am J Respir Cell Mol Biol*. 50(2):419–428.
29 Bird AD, McDougall AR, Seow B, Hooper SB, Cole TJ. 2015. Glucocorticoid regulation of lung development: lessons learned from conditional GR knockout mice. *Mol Endocrinol*. 29(2):158–171.
30 Mobius MA, *et al.* 2019. Oxygen disrupts human fetal lung mesenchymal cells. Implications for bronchopulmonary dysplasia. *Am J Respir Cell Mol Biol*. 60(5):592–600.
31 McDougall AR, *et al.* 2011. The oncogene Trop2 regulates fetal lung cell proliferation. *Am J Physiol Lung Cell Mol Physiol*. 301(4): L478–L489.
32 Van Moortel L, *et al.* 2024. Selective modulation of the human glucocorticoid receptor compromises GR chromatin occupancy and recruitment of p300/CBP and the mediator complex. *Mol Cell Proteomics*. 23(3):100741.
33 Bruno NE, *et al.* 2021. Chemical systems biology reveals mechanisms of glucocorticoid receptor signaling. *Nat Chem Biol*. 17(3): 307–316.

34 Manley BJ, *et al.* 2023. Intratracheal budesonide mixed with surfactant to increase survival free of bronchopulmonary dysplasia in extremely preterm infants: study protocol for the international, multicenter, randomized PLUSS trial. *Trials*. 24(1):320.

35 Pofi R, Caratti G, Ray DW, Tomlinson JW. 2023. Treating the side effects of exogenous glucocorticoids; can we separate the good from the bad? *Endocr Rev*. 44(6):975–1011.

36 Kuna P, *et al.* 2017. Efficacy and tolerability of an inhaled selective glucocorticoid receptor modulator—AZD5423—in chronic obstructive pulmonary disease patients: phase II study results. *Basic Clin Pharmacol Toxicol*. 121(4):279–289.

37 Brown MN, *et al.* 2019. Efficacy and safety of AZD7594, an inhaled non-steroidal selective glucocorticoid receptor modulator, in patients with asthma: a phase 2a randomized, double blind, placebo-controlled crossover trial. *Respir Res*. 20(1):37.

38 van Laar JM, *et al.* 2023. AZD9567 versus prednisolone in patients with active rheumatoid arthritis: a phase IIa, randomized, double-blind, efficacy, and safety study. *Clin Transl Sci*. 16(12):2494–2506.

39 Guglieri M, *et al.* 2022. Efficacy and safety of vamorolone vs placebo and prednisone among boys with duchenne muscular dystrophy: a randomized clinical trial. *JAMA Neurol*. 79(10):1005–1014.

40 Heier CR, *et al.* 2013. VBP15, a novel anti-inflammatory and membrane-stabilizer, improves muscular dystrophy without side effects. *EMBO Mol Med*. 5(10):1569–1585.

41 Liu X, *et al.* 2020. Disruption of a key ligand-H-bond network drives dissociative properties in vamorolone for Duchenne muscular dystrophy treatment. *Proc Natl Acad Sci U S A*. 117(39): 24285–24293.

42 Ruegger CM, Bassler D. 2019. Alternatives to systemic postnatal corticosteroids: inhaled, nebulized and intratracheal. *Semin Fetal Neonatal Med*. 24(3):207–212.

43 Clouse BJ, SR J, Slaughter JL. 2016. Systematic review of inhaled bronchodilator and corticosteroid therapies in infants with bronchopulmonary dysplasia: implications and future directions. *PLoS One*. 11(2):e0148188.

44 Bassler D, *et al.* 2018. Long-term effects of inhaled budesonide for bronchopulmonary dysplasia. *N Engl J Med*. 378(2):148–157.

45 Daley-Yates PT. 2015. Inhaled corticosteroids: potency, dose equivalence and therapeutic index. *Br J Clin Pharmacol*. 80(3):372–380.

46 Auger JP, *et al.* 2024. Metabolic rewiring promotes anti-inflammatory effects of glucocorticoids. *Nature*. 629(8010):184–192.

47 McNamara PJ, Alcorn J. 2002. Protein binding predictions in infants. *AAPS PharmSci*. 4(1):E4.

48 Ryrfeldt A, *et al.* 1982. Pharmacokinetics and metabolism of budesonide, a selective glucocorticoid. *Eur J Respir Dis Suppl*. 122: 86–95.

49 Raaska K, Niemi M, Neuvonen M, Neuvonen PJ, Kivisto KT. 2002. Plasma concentrations of inhaled budesonide and its effects on plasma cortisol are increased by the cytochrome P4503A4 inhibitor itraconazole. *Clin Pharmacol Ther*. 72(4):362–369.

50 Esmailpour N, Hogger P, Rohdewald P. 1998. Binding kinetics of budesonide to the human glucocorticoid receptor. *Eur J Pharm Sci*. 6(3):219–223.

51 McDougall AR, *et al.* 2013. Trop2 regulates motility and lamellipodia formation in cultured fetal lung fibroblasts. *Am J Physiol Lung Cell Mol Physiol*. 305(7):L508–L521.

52 Pipkin ME, *et al.* 2010. Interleukin-2 and inflammation induce distinct transcriptional programs that promote the differentiation of effector cytolytic T cells. *Immunity*. 32(1):79–90.

53 Kim D, Paggi JM, Park C, Bennett C, Salzberg SL. 2019. Graph-based genome alignment and genotyping with HISAT2 and HISAT-genotype. *Nat Biotechnol*. 37(8):907–915.

54 Danecek P, *et al.* 2021. Twelve years of SAMtools and BCFtools. *Gigascience*. 10(2):giab008.

55 Anders S, Pyl PT, Huber W. 2015. HTSeq–a Python framework to work with high-throughput sequencing data. *Bioinformatics*. 31(2):166–169.

56 Robinson MD, McCarthy DJ, Smyth GK. 2010. Edger: a Bioconductor package for differential expression analysis of digital gene expression data. *Bioinformatics*. 26(1):139–140.

57 Xie Z, *et al.* 2021. Gene set knowledge discovery with Enrichr. *Curr Protoc*. 1(3):e90.

58 Trott O, Olson AJ. 2010. AutoDock Vina: improving the speed and accuracy of docking with a new scoring function, efficient optimization, and multithreading. *J Comput Chem*. 31(2):455–461.

59 Roe DR, Cheatham TE 3rd. 2013. PTRAJ and CPPTRAJ: software for processing and analysis of molecular dynamics trajectory data. *J Chem Theory Comput*. 9(7):3084–3095.

60 Grant BJ, Rodrigues AP, ElSawy KM, McCammon JA, Caves LS. 2006. Bio3d: an R package for the comparative analysis of protein structures. *Bioinformatics*. 22(21):2695–2696.